Metal−Insulator Transition Induced by Ce Doping in $CaMnO_3$

M. E. Melo Jorge,*,† M. R. Nunes,† R. Silva Maria,† and D. Sousa‡

Departamento de Química e Bioquímica/CCMM, Faculdade de Ciências, Universidade de Lisboa, Campo Grande, 1749-016 Lisboa, Portugal, and CCMM, Faculdade de Ciências, Universidade de Lisboa, Campo Grande, 1749-016 Lisboa, Portugal

Received August 3, 2004. Revised Manuscript Received December 1, 2004

Study of the perovskite-type manganites $Ca_{1-x}Ce_xMnO_3$ ($0.00 \leq x \leq 0.25$) has been carried out. The electrical resistivity values for these samples were measured in the temperature range from 300 up to 900 K and show that the doping of the phase $CaMnO_3$ with cerium induces simultaneously a marked decrease in the electrical resistivity and a metal-to-insulator transition. This behavior is exceptional since such a transition has not been observed to date in these compounds for these experimental conditions and can be attributed to the formation of Mn^{3+} ions as a result of charge compensation. The values of metal-to-insulator transition temperature, T_{MI}, change with Mn^{3+} amount. Further the carrier doping tends to suppress the semiconductor behavior of $CaMnO_3$ and the T_{MI} is attributed to charge ordering observed in these compounds around 255 K.

Introduction

Discovery of colossal magnetoresistance (CMR) and extraordinary richness of the transport properties in mixed valence compounds with general formula $Ln_{1-x}A_xMnO_3$ (Ln = rare earth, A = alkaline earth) promoted an intensive study of these type of compounds in the last few years. Some of these perovskites exhibit fascinating properties such as metal−insulator (M−I) transitions, charge ordering, and ferromagnetism.[1−7] The double exchange mechanism,[8] controlled by the motion of the e_g electrons from Mn^{3+} to Mn^{4+} sites, is used to explain the ferromagnetic behavior of these phases, while the simultaneous presence of ferromagnetism and metallic state brings about magnetoresistance when the magnetic field is changed.[9−11]

So far, most of the studies had been concentrated on the hole-doped manganites. In contrast, there are only a few reports on the electron-doped materials, corresponding to compositions with high content of Mn^{4+} ions. Magnetic study of the $Ca_{1-x}Eu_xMnO_3$ ($0 < x < 1$) perovskites has been studied by Troyanchuk el al.[12] In $Bi_{1-x}Ca_xMnO_3$ ($x \geq 0.8$) a ferromagnetic moment and reduced resistivity are observed and also a negative magnetoresistance appears below T_C.[13] In the case of $Ca_{1-x}Sm_xMnO_3$ ($x \leq 0.2$)[4] CMR properties are exhibited for $x = 0.15$, and for $Ca_{1-x}A_xMnO_3$ (A = Pr, Nd, Eu, Gd, Ho, Ce, Th),[14] prepared by traditional solid-state methods, the authors observed a large magnetoresistance. In fact, the authors argued that the CMR effect in these electron-doped manganites appears in a very narrow range of carrier concentration with unusual effects of the variation of the average size of the ions at the rare earth site. Recently, Zeng et al.[15] and Caspi et al.[16] reported the structural and the magnetic and transport measurements of $Ca_{1-x}Ce_xMnO_3$ ($x \leq 0.2$) system, synthesized by sol−gel method, but only for below 400 K.[15] The XAS results indicate that the formal oxidation state of cerium is Ce^{4+}, the Ce-doping leads to mixed valence Mn^{3+} and $Mn^{4,+}$ and a large magnetoresistance was observed for the $Ca_{0.925}Ce_{0.075}MnO_3$ phase.

On the other hand, the electrical transport properties of $(Ca_{0.9}M_{0.1})MnO_3$ (M = Y, La, Ce, Sm, In, Sn, Sb, Pb, Bi), prepared by ceramic methods, were investigated by Ohtaki et al.[17] They reported that the substitution at the Ca site causes an increase in the electrical conductivity attributed at least partly to an increase in the carrier concentration caused by doping effect of the higher valence cations. Moreover, they observed a negative linear relation when log-

* Corresponding author. E-mail: mebmj@fc.ul.pt.
† Departamento de Química e Bioquímica/CCMM.
‡ CCMM.

(1) von Helmot, R.; Wecker, J.; Holzapfel, B.; Schultz L.; Samwer, K. *Phys. Rev. Lett.* **1993**, *71*, 2331.
(2) Mahesh, R.; Mahendiran, R.; Raychaudhuri A. K.; Rao, C. N. R. *J. Solid State Chem.* **1995**, *114*, 297.
(3) Raveau, B.; Maignan A.; Martin, C. *J. Solid State Chem.* **1997**, *130*, 162.
(4) Martin, C.; Maignan, A.; Damay, F.; Hervieu M.; Raveau, B. *J. Solid State Chem.* **1997**, *134*, 198.
(5) Rao, C. N. R.; Mahesh, R. *Curr. Opin. Solid State Mater Sci.* **1997**, *2*, 32.
(6) Rao, C. N. R.; Santosh, A. P. N.; Cheetham, A. K. *Chem. Mater.* **1998**, *10*, 2714.
(7) Dagotto, E.; Hotta T.; Moreo, A. *Phys. Rep.* **2000**, *344*, 1.
(8) Zenner, C. *Phys. Rev.* **1951**, *82*, 403.
(9) Jin, S.; Tiefel, T. H.; McCormack, M.; Fastnacht, R. A.; Ramesh, R.; Chen, J. H. *Science* **1994**, *264*, 413.
(10) De Teresa, J. M.; Ibarra, M. R.; Algarabel, P. A.; Ritter, C.; Marquina, C.; Blasco, J.; Garcia, J.; Moral, A. del; Arnold, Z. *Nature* **1997**, *386*, 256.
(11) Varma, C. M. *Phys. Rev. B* **1996**, *54*, 7328.
(12) Troyanchuk, I. O.; Samsonenko, N. V. *J. Solid State Chem.* **1997**, *131*, 144.
(13) Chiba, H.; Kikuchi, M.; Kusaba, K.; Muraoka, Y.; Syono, Y. *Solid State Commun.* **1996**, *99*, 499.
(14) Maignan, A.; Martin, C.; Damay, F.; Raveau, B. *Chem. Mat.* **1998**, *10*, 950.
(15) Zeng, Z.; Greenblatt, M.; Croft, M. *Phys. Rev. B.* **2001**, *63*, 224410−1.
(16) Caspi, E. N.; Avdeev, M.; Short, S.; Jorgensen, J. D.; Lobanov, M. V.; Zeng, Z.; Greenblatt, M.a; Thiyagarajan, P.; Botez, C. E.; Stephens, P. W. *Phys. Rev. B* **2004**, *69*, 104402−1.
(17) Ohtaki, M.; Kiga, H.; Tokunaga, T.; Eguchi, K.; Arai, H. *J. Solid State Chem.* **1995**, *120*, 105.

10.1021/cm040188b CCC: $30.25
Published on Web 03/18/2005

(σT) was plotted against $1/T$ for some phases, indicating that hopping conduction mechanism occurs in these oxides.

Also, many investigations have been reported on the substitution of Ca^{2+} by other rare earth ions in orthorhombic perovskite-type $CaMnO_3$.[18−21] The electrical resistivity measurements of $(Ln_{1-x}Ca_x)MnO_3$ (Ln = La, Nd, Gd, Th, Ho, Y) indicate that all manganites are n-type semiconductors at low temperature and exhibit a metal−insulator transition at high temperature without any crystallographic variation.

In this paper, we report a detailed study on the structural and electrical properties of the electron-doped manganites $Ca_{1-x}Ce_xMnO_3$ ($x \leq 0.25$) to study the correlation between structural parameters and metal−insulator transition at high temperature. These results provide information for the discussion of the behavior of the 3d electrons of Mn ions in the conduction mechanism of this perosvkite-type oxide system.

Experimental Section

Samples of $Ca_{1-x}Ce_xMnO_3$ ($x \leq 0.25$) were prepared by the nitrate−citrate sol−gel technique. Appropriate amounts of $CaCO_3$ (Aldrich, >99.995%), $(NH_4)_2Ce(NO_3)_6$ (Riedel-de Haën, p.a.), and $Mn(NO_3)_2 \cdot 4H_2O$ (Riedel-de Haën, p.a.) were separately dissolved in a HNO_3 (Merck, p.a.) solution, prior to mixture, that was followed by the addition of citric acid (Merck, p.a.). The solution was slowly evaporated and dried on a hot plate for about 2−3 h. The formed powder was then decomposed in an evaporating dish at 873 K for 6 h to decompose the organic compounds. The resulting amorphous powder for $x \leq 0.10$ was ground and heated in air at 1073 K for 54 h with intermediate grinding and then annealed again at 1123 K for 18h. For $0.15 \leq x \leq 0.25$ the amorphous powder was first heated to 1373 K for 54 h then annealed up to 1423 K ($x = 0.15$) and 1473 K ($x \geq 0.20$) for 36 h, and then slowly cooled to room temperature. All the thermal treatments were performed in alumina crucibles (Alsint 99.7).

X-ray powder diffraction (XRD) was carried out for all samples, using a Philips PW 1730 X-ray powder diffractometer, operating with monochromatized Cu Kα radiation and scanning (0.02° step in 2θ) over the range $20° \leq 2\theta \leq 120°$. Lattice parameters were first refined by a least-squares method. The final powder diffraction data were analyzed using the Rietveld method, with the FullProf program.[22]

Morphological observations of the samples were performed by scanning electron microscopy (SEM) using a JEOL (JSM-35C).

The electrical resistivity measurements were carried out with a standard four-probe technique in the temperature range of 298−873 K.

Results and Discussion

Structural and Morphological Characterization. Although in a recent work,[16] it has been referred from neutron and X-ray diffraction data that the $Ca_{1-x}Ce_xMnO_3$ system with $0.1 \leq x \leq 0.167$ exhibits a monoclinic structure with very small angle that changes between $90.088(4) \leq \beta \leq 90.189$, our results present a better fitting considering the *Pnma* space group (orthorhombic structure). It is important to note that the heat treatments for our samples were slightly different from the published one, i.e., longer periods of time and higher temperature values were used in our samples. During these treatments the crystallinity of the samples was improved and a better definition of the peak shape of XDR data was observed. The Rietveld refinement XRD patterns of all samples were carried out considering an orthorhombic structure. Attempts to refine the XRD data with the monoclinic structure, as previously referred, did not allow improvement of the fittings. It has to be highlighted that the lattice parameters of the monoclinic cell previously reported[16] indicate a slight distortion from the orthorhombic structure, a fact that can justify the difficulty in improving the refinements considering this symmetry. For these reasons, in this work a structure analysis of these compounds based on the orthorhombic structure is presented; although the symmetry is possibly $P2_1/m$ for $x \geq 0.1$ samples the resolution of the data does not allow the confirmation of that space group symmetry.

Hence, at room temperature the Rietveld refinement XRD patterns show that the samples for all compositions are single-phase with orthorhombically distorted perovskite-type structure (*Pnma* space group). Background Rietveld refinements were fitted with a polynomial function; a pseudo-Voigt function was employed to model the peak shape and two asymmetry parameters were used. The initial positional parameters were taken from previously reported data of the $CaMnO_3$ phase[23−25] and isotropic temperature factors were fixed at 0.01 Å^2. All reflections could be indexed as the orthorhombic perovskite-type structure and a good level of agreement between the observed and calculated XRD patterns for all samples was obtained. The X-ray diffraction patterns, including the raw data, the global fitted profile, and the differences for two representative members of the series with $x = 0$ and $x = 0.25$ are shown in Figure 1.

Structural refinements of the XRD data, namely the cell parameters, atomic positions, and fitting results are presented in Table 1 for all phases. In Table 2 we present the Mn−O bond distances, average equatorial bond length ⟨Mn−O(2)⟩, average bond length ⟨Mn−O(oct)⟩ and Mn−O−Mn bond angles calculated from these results. For a better analysis of the results the D values (D = Mn−O(1)/⟨Mn−O(2)⟩) are also included in the Table 2.

The XRD pattern of $Ca_{1-x}Ce_xMnO_3$ ($x \leq 0.25$) exhibits the orthorhombic $GdFeO_3$ structure with cell parameters $a \approx a_p\sqrt{2}$, $b \approx 2a_p$, $c \approx a_p\sqrt{2}$ (with a_p referring to the lattice parameter for the ideal cubic perovskite structure). Figure 2 shows the variation of the lattice parameters as a function of the Ce concentration, where $b/\{\sqrt{2}\}$ has also been shown. It can readily be seen that the following relations

(18) Taguchi, H.; Nagao, M.; Shimada, M. *J. Solid State Chem.* **1988**, *76*, 284.
(19) Taguchi, H.; Nagao, M.; Shimada, M. *J. Solid State Chem*. **1989**, *82*, 8.
(20) Kobayashi, T.; Takizawa, H.; Endo, T.; Sato, T.; Shimada, M.; Taguchi, H. Nagao, M. *J. Solid State Chem.* **1991**, *92*, 116.
(21) Taguchi, H., Shimada, M. *J. Solid State Chem.* **1986**, *63*, 290.
(22) Rodriguez-Carvajal, J. FullProf, version 1.8a − May 2002. ILL (unpublished).
(23) Poeppelmeier, K. R.; Leonowicz, M. E.; Scanlon, J. C.; Longo, J. M. *J. Solid State Chem.* **1982**, *45*, 71.
(24) Melo Jorge, M. E.; dos Santos, A. C.; Nunes, M. R. *Int. J. Inorg. Mater.* **2001**, *3*, 915.
(25) Fawcett, I. D.; Sunstrom, J. E.; Greenblatt, M.; Croft, M.; Ramanujachary, K. V. *Chem. Mater*. **1998**, *10*, 3643.

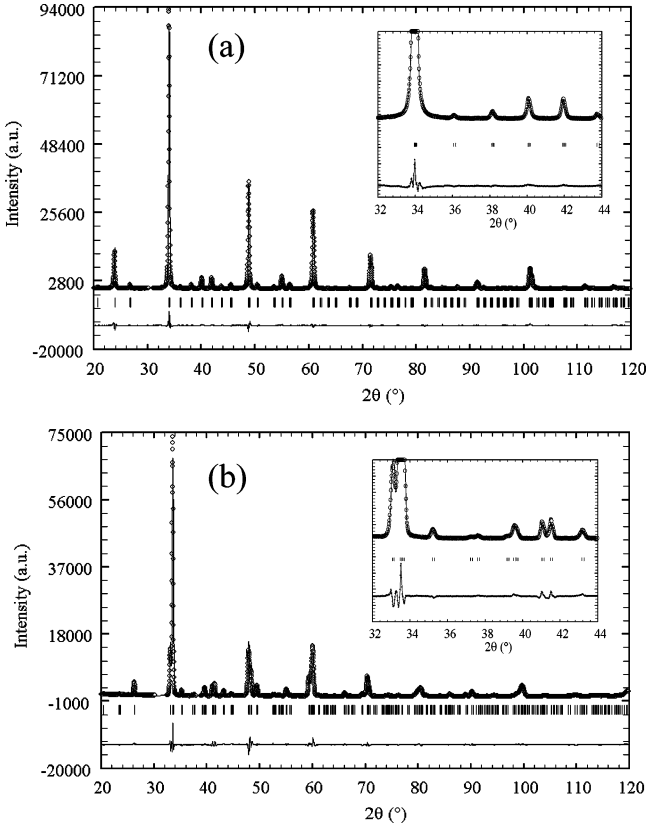

Figure 1. Rietveld refinement results for $CaMnO_3$ and $Ca_{0.75}Ce_{0.25}MnO_3$. The experimental data points are shown as dots, and the calculated fit and difference curve are shown as solid lines. Tick marks indicate the calculated reflection positions. The inset shows a zoom in region between 32 and 44° (2θ). (a) $x = 0.00$, (b) $x = 0.25$.

$\{b\}/\{\sqrt{2} > c\}$ and $c < a$ take place below $x = 0.05$, and so the perovskite lattice of each these phases is an O-type orthorhombic structure. For the other compositions $0.10 \leq x \leq 0.25$ the relation $b/\{\sqrt{2}\} < c < a$ is valid and the orthorhombic cell is referred as O′-type structure[2626] and it can be originated by the strong cooperative Jahn-Teller effect, inducing a distortion of the MnO_6 octahedra preferentially occurring for Mn−O(2) rather than Mn−O(1), as recently reported.[27]

All lattice parameters increase with Ce substitution on the A-site and this increase is more significant in the $a-c$ plane (Figure 2); as a consequence, the orthorhombicity factor a/c increases strongly and the unit-cell volume also shows a progressive expansion. This effect is easily understood since the Ce substitution for Ca leads to an increased concentration of Mn^{3+} (0.645 Å) in the structure, which is larger than Mn^{4+} (0.530 Å).[28] In recent studies of several $Ca_{1-x}Ce_xMnO_3$ phases, the authors[14,15] concluded that cerium is tetravalent. Although the effective ionic radius of Ce^{4+} (1.14 Å) is smaller than that of Ca^{2+} (1.34 Å) and considering stoichiometric phases, we can conclude that the increase of the mean ionic radius of the B site (10.9%) is higher than the decrease of the mean ionic radius of the A site (3.7%) as can be seen in Table 3. So an expansion of the cell volume was comprehensible. The global results for the undoped and doped samples are in excellent agreement with the previously reported results.[14,15,23−25]

On the other hand the tolerance factor (t), which is a quantitative measure of the structural perfection of the ABO_3 perovskites, was calculated by using the average values for r_A and r_B and these values are also presented in the Table 3. The t values reflect the effects of replacement of Ca^{2+} for Ce^{4+} ions in the series $Ca_{1-x}Ce_xMnO_3$. Decreasing the Ce content the tolerance factor approaches the ideal value ($t \rightarrow 1$) and the tilting of the (MnO_6) octahedra are significantly lower in comparison with the phases containing high concentrations of cerium. As was referred previously with increasing Ce concentration, the average A site ion size, $\langle r_A \rangle$, decreases by 3.7% and the $\langle r_B \rangle$ increases by 10.9%. Both effects result in a decrease of the tolerance factor by 4.3%. A decrease in value of t leads to a significant lowering in the Mn−O−Mn bond angle from 180°. The major effect on t, and therefore in the Mn−O−Mn bond angle, is the increase in the MnO_6 polyhedral size as we can see from the average bond lengths of octhaedra ⟨Mn−O(oct)⟩ included in Table 2. From this table we can observe a systematic change in the values of the bond length and the bond angle with Ce composition as the lattice parameters increase with Ce content. For the $x = 0$ phase the Mn−O distances and bond angles can be compared with the corresponding values reported for the same phase.[23−25] For the doped samples, consistent with the increase of all cell lattices, we find that the Mn−O bond lengths show a gradual increase with Ce content. This effect is more clearly seen along the $a-c$ basal plane, as changes in Mn−O(2) bonds lengths. The change on the apical-bond length Mn−O(1) is much smaller compared to the $a-c$ basal plane (see Figure 3). In general, for the undoped sample the octahedral coordination of manganese with oxygen is almost undistorted, with six approximately equal Mn−O distances. For the doped samples the four Mn−O(2) distances in the $a-c$ plane become longer than the two Mn−O(1) distances along the b axis, since in this case the JT distortion perturbed by the Mn^{3+} content mainly affects the equatorial Mn−O(2) bonds. The increase of the distortion structure with Ce content is also well visible by the systematic decrease of the octahedral distortion parameter values D (Table 2). Moreover, as cerium content increases, the Mn−O(1)−Mn and Mn−O(2)−Mn angles indicate a higher distortion. For $x = 0$ both angles are similar and close to 160° and become significantly different from each other and smaller than 160° as Ca is substituted by Ce.

Scanning electron micrographs for all samples presented in Figure 4 reveal that morphology of the cerium-substituted samples with $x = 0.01$ and 0.05 is more or less similar. Beyond $x = 0.05$ a significant increase in particle size with increasing Ce content is observed, and this morphological change is essentially due to the increased extent of substitution of cerium and to the annealing conditions for $x \geq 0.15$ (higher temperature and longer duration relative to other samples with $x \leq 0.10$).

Electrical Resistivity. The temperature dependence of resistivity of $Ca_{1-x}Ce_xMnO_3$ samples is shown in Figure 5. The inspection of this figure clearly shows that doping the

(26) Goodenough, J. B., Longo, L. M. *Crystallographic and Magnetic Properties of Perovskite and Perovskite-Related Compounds*; Landolt-Bornstein Tabellen, New Series III/4a; Springer-Verlag: Berlin, 1970.
(27) Lufaso, M. W.; Woodward, P. M. *Acta Crystallogr.* **2004**, *B60*, 10.
(28) Shannon, R. D. *Acta Crystallogr.* **1976**, *A32*, 751.

Table 1. Refined Structural Parameters for $Ca_{1-x}Ce_xMnO_3$ in an Orthorhombic (*Pnma*) Unit Cell

	atom	site	*x*	*y*	*z*
$CaMnO_3$	Ca	4c	0.0323 (3)	0.25	−0.0093 (1)
a = 5.2791 (2) (Å)	Mn	4b	0	0	0.5
b = 7.4566 (2) (Å)	O(1)	4c	0.4932 (4)	0.25	0.0683 (4)
c = 5.2706 (2) (Å)	O(2)	8d	0.2904 (3)	0.0302 (3)	−0.2890 (3)
V = 207.47 (1) (Å^3)			Rwp = 8.52%	R_B = 2.41%	R_F = 2.81%
$Ca_{0.99}Ce_{0.01}MnO_3$	Ca/Ce	4c	0.0317 (1)	0.25	−0.0097 (1)
a = 5.2863 (2) (Å)	Mn	4b	0	0	0.5
b = 7.4624 (3) (Å)	O(1)	4c	0.4915 (4)	0.25	0.0694 (4)
c = 5.2737 (2) (Å)	O(2)	8d	0.2901 (3)	0.0305 (3)	−0.2886 (3)
V = 208.04 (1) (Å^3)			Rwp = 8.86%	R_B = 2.41%	R_F = 2.71%
$Ca_{0.95}Ce_{0.05}MnO_3$	Ca/Ce	4c	0.0314 (1)	0.25	−0.0070 (1)
a = 5.3041 (2) (Å)	Mn	4b	0	0	0.5
b = 7.4787 (3) (Å)	O(1)	4c	0.4880 (4)	0.25	0.0682 (4)
c = 5.2852 (2) (Å)	O(2)	8d	0.2894 (3)	0.0338 (3)	−0.2891 (4)
V = 209.65 (1) (Å^3)			Rwp = 7.65%	R_B = 2.20%	R_F = 2.99%
$Ca_{0.90}Ce_{0.10}MnO_3$	Ca/Ce	4c	0.0328 (3)	0.25	−0.0092 (1)
a = 5.3242 (2) (Å)	Mn	4b	0	0	0.5
b = 7.4898 (3) (Å)	O(1)	4c	0.4849 (4)	0.25	0.0684 (4)
c = 5.2972 (2) (Å)	O(2)	8d	0.2913 (3)	0.0341 (3)	−0.2909 (3)
V = 211.24 (1) (Å^3)			Rwp = 8.27%	R_B = 2.79%	R_F = 3.17%
$Ca_{0.85}Ce_{0.15}MnO_3$	Ca/Ce	4c	0.0364 (2)	0.25	−0.0098 (1)
a = 5.3534 (1) (Å)	Mn	4b	0	0	0.5
b = 7.5033 (2) (Å)	O(1)	4c	0.4897 (4)	0.25	0.0691 (4)
c = 5.3115 (1) (Å)	O(2)	8d	0.2910 (2)	0.0356 (2)	−0.2907 (2)
V = 213.35 (1) (Å^3)			Rwp = 9.80%	R_B = 3.48%	R_F = 3.74%
$Ca_{0.80}Ce_{0.20}MnO_3$	Ca/Ce	4c	0.0388 (1)	0.25	−0.0093 (1)
a = 5.3793 (2) (Å)	Mn	4b	0	0	0.5
b = 7.5135 (3) (Å)	O(1)	4c	0.4898 (5)	0.25	0.0715 (5)
c = 5.3230 (2) (Å)	O(2)	8d	0.2916 (3)	0.0374 (3)	−0.2917 (3)
V = 215.14 (1) (Å^3)			Rwp = 10.9%	R_B = 3.78%	R_F = 3.83%
$Ca_{0.75}Ce_{0.25}MnO_3$	Ca/Ce	4c	0.0429 (1)	0.25	−0.0095 (1)
a = 5.4140 (2) (Å)	Mn	4b	0	0	0.5
b = 7.5338 (3) (Å)	O(1)	4c	0.4906 (6)	0.25	0.0734 (6)
c = 5.3295 (2) (Å)	O(2)	8d	0.2895 (3)	0.0421 (3)	−0.2901 (3)
V = 217.38 (1) (Å^3)			Rwp = 11.8%	R_B = 4.38%	R_F = 3.68%

Table 2. Selected Bond Distances (Å), Angles (Degrees), and *D* Values from Rietveld Refinements for $Ca_{1-x}Ce_xMnO_3$ ($0 \le x \le 0.25$)

x	0	0.01	0.05	0.1	0.15	0.2	0.25
Mn −O(1)	1.899 (1) × 2	1.902 (1)	1.905 (1)	1.909 (1)	1.912 (1)	1.917 (1)	1.924 (1)
Mn −O(2)	1.907 (2) × 2	1.910 (2)	1.914 (2)	1.923 (2)	1.932 (1)	1.941 (2)	1.952 (2)
	1.896 (2) × 2	1.897 (2)	1.910 (2)	1.917 (2)	1.925 (1)	1.936 (2)	1.947 (2)
⟨Mn−O(2)⟩	1.902	1.903	1.912	1.920	1.928	1.938	1.950
⟨Mn−O(oct)⟩	1.901	1.903	1.910	1.916	1.923	1.931	1.941
D[a]	0.998	0.999	0.996	0.994	0.992	0.989	0.987
Mn−O(1)−Mn	158.04 (2)	157.65 (2)	157.86 (2)	157.56 (2)	157.60 (2)	156.84 (2)	156.33 (3)
Mn−O(2)−Mn	157.44 (7)	157.46 (7)	156.59 (6)	155.91 (7)	155.59 (6)	154.84 (7)	154.01 (8)

[a] D = Mn−O(1)/⟨Mn−O(2)⟩.

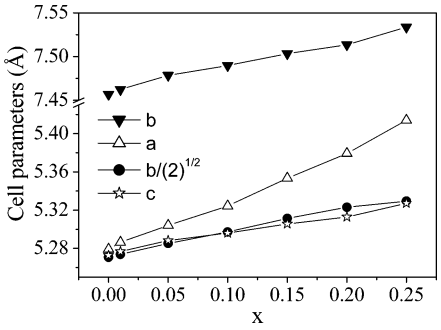

Figure 2. Cell parameters of the $Ca_{1-x}Ce_xMnO_3$ manganites ($x \le 0.25$) plotted vs *x* (Ce content).

calcium site with cerium rapidly and significantly lowers the resistivity by several orders of magnitude with respect to $CaMnO_3$, and the behavior of the Ce-doped phase is much different. For the Ce-doped phases the electrical resistivity values at 300 K (ρ_{300K}) decrease significantly up to $x = 0.15$, then increase slightly for $x = 0.25$. Hence the composition $x = 0.15$ shows the maximum electrical conductivity (see Figure 5 and Table 4). The origin of this reduction of resistivity should be attributed to the systematic change in structural parameters and in the valence state of Mn with calcium substitution. So the presence of an appreciable concentration of Mn^{3+} introduces a large number of charge carriers (electron) and facilitates the movement of those charge carriers by hopping mechanism.

These results are similar to the ones reported by Iwahara et al.,[29] although they obtained higher electronic conductivity values from room temperature to 1373 K.

(29) Iwahara, H., Esaka, T., Hamajima, H., *Denki Kagaku* **1989**, *57*, 591.

Table 3. Ionic Composition, Mean Ionic Radius of the A and B Sites, and the Tolerance Factor (t) for $Ca_{1-x}Ce_xMnO_3$

x	(Ca, Ce)$Mn^{4+}_{1-y}\,Mn^{3+}_{y}\,O_3$	Mean ionic radius (A site − XII) (Å)	Mean ionic radius (B site − VI) (Å)	t
0.00	$CaMan^{4+}\,O_3$	1.34	0.530	1.004
0.01	$Ca_{0.99}Ce_{0.01}Mn^{4+}_{0.98}\,Mn^{3+}_{0.02}\,O_3$	1.34	0.532	1.003
0.05	$Ca_{0.95}Ce_{0.05}Mn^{4+}_{0.90}\,Mn^{3+}_{0.10}\,O_3$	1.33	0.542	0.994
0.10	$Ca_{0.90}Ce_{0.10}Mn^{4+}_{0.80}\,Mn^{3+}_{0.20}\,O_3$	1.32	0.553	0.985
0.15	$Ca_{0.85}Ce_{0.15}Mn^{4+}_{0.70}\,Mn^{3+}_{0.30}\,O_3$	1.31	0.564	0.976
0.20	$Ca_{0.80}Ce_{0.20}Mn^{4+}_{0.60}\,Mn^{3+}_{0.40}\,O_3$	1.30	0.576	0.966
0.25	$Ca_{0.75}Ce_{0.25}Mn^{4+}_{0.50}\,Mn^{3+}_{0.50}\,O_3$	1.29	0.588	0.957

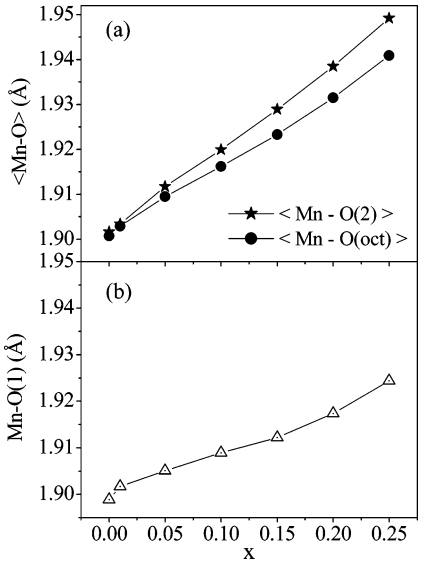

Figure 3. Average ⟨Mn−O⟩ bond length (a) and Mn−O(1) bond distance (b) as a function of x in $Ca_{1-x}Ce_xMnO_3$ ($x \leq 0.25$).

Also the values of the room-temperature resistivity (ρ_{RT}), previously reported for $Ca_{1-x}Ce_xMnO_3$ samples ($x \leq 0.2$),[15] agree with the values measured in the present work. On the other hand, at the high-temperature region the electrical behavior for our system $Ca_{1-x}Ce_xMnO_3$ is very different from that of $La_{1-x}Ca_xMnO_3$ thin films[30] for lower x values. For instance, the electron-doped manganites $Ca_{1-x}Ce_xMnO_3$ exhibit a metallic behavior in the range 300−900 K and a metal−insulator transition for $0.01 \leq x \leq 0.25$, whereas the hole-doped manganites $La_{1-x}Ca_xMnO_3$ exhibit insulating properties from 300 to 1200 K. In $La_{1-x}Ca_xMnO_3$ as x increases the resistivity drops 3 orders of magnitude and then, at room temperature, reaches a minimum for $x = 0.83$ ($La_{0.17}Ca_{0.83}MnO_3$). Furthermore, the detailed study of $Sm_{1-x}Ca_xMnO_3$[31] with $0.3 \leq x \leq 1$ between 10 and 320 K revealed that when the calcium concentration is increased the transport properties gradually change; metallic-like variation starts to dominate the temperature dependence of resistivity and the ρ_{300K} value was minimum also for $x = 0.85$.

For $x = 0$ the $\rho(T)$ curve (inset of Figure 5) is characteristic of semiconducting sample ($\{d\rho\}/\{dT\} < 0$) in the whole temperature range. Moreover, except for $x = 0.15$, the $\rho(T)$ curves show a metal−insulator transition for all phases marked by the presence of a broad peak in the resistivity curves. One observes that with increment of x, the temperature transition, T_{MI}, taken at the inflection point, first decreases from about 607 K (for $x = 0.01$), reaches the values 327 K for $x = 0.10$ and 328 K for $x = 0.20$, and then for higher x values ($x = 0.25$) T_{MI} increases up to 413 K (see Figure 5 and Table 4). The $Ca_{0.99}Ce_{0.01}MnO_3$ sample shows a slope change at the metal−insulator transition, exhibiting a broad peak transition, while $Ca_{0.95}Ce_{0.05}MnO_3$ and $Ca_{0.75}Ce_{0.25}MnO_3$ phases show a significantly smaller increase in the resistivity upon cooling below the transition. The resistivity of the intermediate values $x = 0.10$ and 0.20 has a small temperature dependence near 300−400 K although a slight change has been observed in the $\rho(T)$ curve at 327−328 K. For $x = 0.15$ there is no visible transition, however a trend to reach a semimetallic state below 300 K can be observed. We can conclude that all doped samples exhibit metallic behavior by cooling from 900 K down reaching a point (depending on the doping level) where the resistivity begins to increase. Below this temperature (T_{MI}) the samples exhibit semiconductor behavior, which is in agreement with the semiconductor behavior reported by Zeng et al.[15] for the electron-doped $Ca_{1-x}Ce_xMnO_3$ ($x \leq 0.20$) samples at a temperature range lower than 300 K.

The trends followed by our data for the high-temperature resistivity of $Ca_{1-x}Ce_xMnO_3$, namely the observation of T_{MI}, are analogous to previous reports on ($Ln_{1-x}Ca_xMnO_3$) (Ln = La, Nd, Ga, Tb, Ho, Y).[18−21] These manganites exhibit a metal−insulator transition at high temperature and the authors adopted the energy band scheme for the perovskite-type structure proposed by Goodenough[32] for the interpretation of the metal−insulator transition. It is concluded that the increase in Mn−O distance enhances the magnitude of the electrostatic field and consequently the transition temperature is raised. In our case this variation is not entirely observed with increasing Mn−O distance. Figure 6 shows a quadratic dependence when T_{MI} is plotted against Mn−O bond length, a minimum is observed between $0.10 \leq x \leq 0.20$. As we can see this dependence is not monotone, other factors must be considered such as charge-ordering phenomenon. In this case, the increase in resistivity below the charge-ordering (CO) transition is typical of many types of CO systems. In previous work,[15,16] for the two electron-doped $Ca_{1-x}Ce_xMnO_3$ system, higher Ce doping ($0.075 \leq x \leq 0.20$) induces a charge orbital ordering transition that increases with composition to near 255 K.

Furthermore, the most important feature concerns the evolution of T_{MI} versus x between our samples and

(30) Worledge, D. C.; Miéville, L.; Geballe, T. H. *Phys. Rev. B* **1998**, *57*, 15267.
(31) Hejtmanek, J.; Jirak, Z.; Marysko, M.; Martin, C.; Maignan, A.; Hervieu M.; Raveau, B. *Phys. Rev. B* **1999**, *60*, 14057.
(32) Goodenough, J. B. *J. Appl. Phys.* **1966**, *37*, 1415.

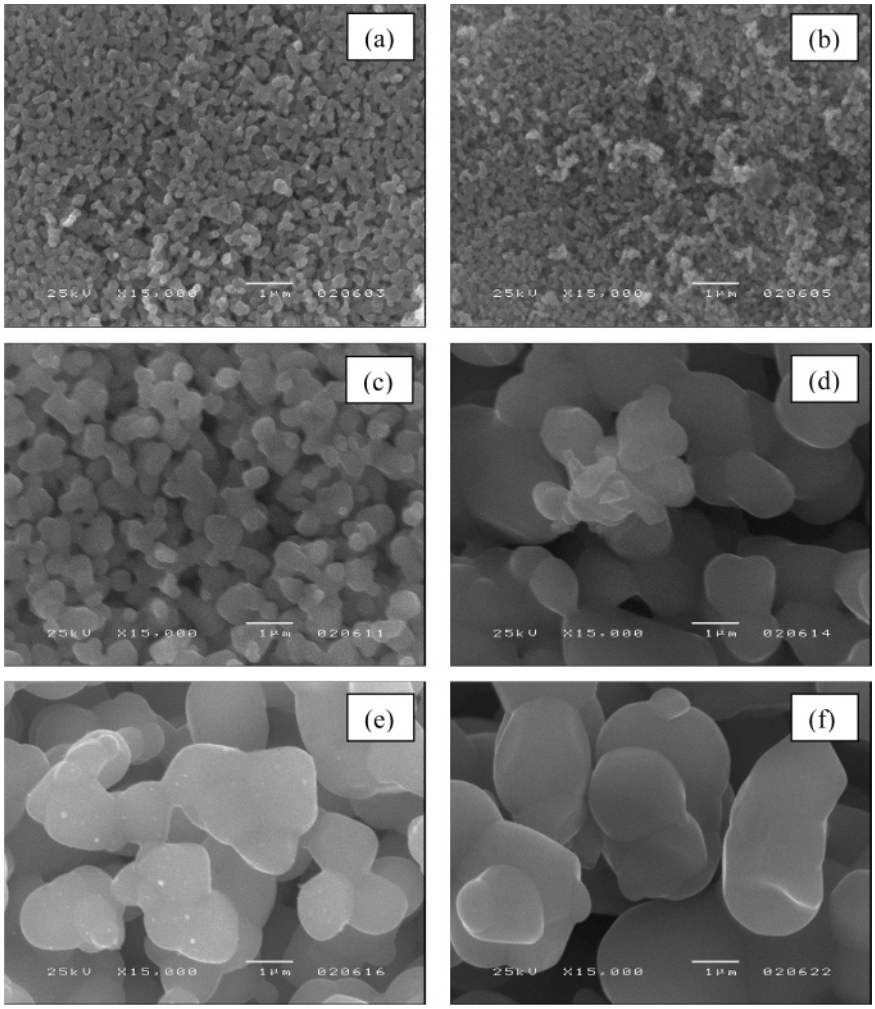

Figure 4. Scanning electron micrographs of $Ca_{1-x}Ce_xMnO_3$ manganites: (a) $x = 0.01$, (b) $x = 0.05$, (c) $x = 0.10$, (d) $x = 0.15$, (e) $x = 0.20$, (f) $x = 0.25$.

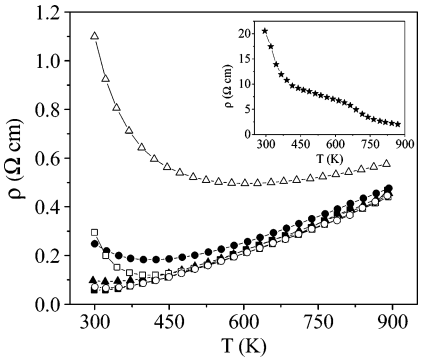

Figure 5. Temperature dependence of the electrical resistivity for $Ca_{1-x}Ce_xMnO_3$ ($0 \le x \le 0.25$). The inset shows the ρ vs T of $CaMnO_3$. (★) $x = 0.00$, (△) $x = 0.01$, (●) $x = 0.05$, (▲) $x = 0.10$, (■) $x = 0.15$, (○) $x = 0.20$, (□) $x = 0.25$.

($Ln_{1-x}Ca_xMnO_3$) (Ln = La, Nd, Ga, Tb, Ho, Y)[18−21] phases. One indeed observes that the T_{MI} corresponding to the metal−insulator transition temperature decreases with increasing cerium content up to $x = 0.15$ and reaches 413 K for $Ca_{0.75}Ce_{0.25}MnO_3$ ($x = 0.25$), whereas for the $Ln_{1-x}Ca_xMnO_3$ ($0.5 \le x \le 0.9$) the T_{MI} decreased gradually with increasing x.[18−20] This difference can be explained by the fact that Ce, due to its tetravalent character, introduces twice as many electrons per atom than trivalent lanthanides ions, according to the chemical formula $Ln_{1-x}Ca_xMn^{3+}_{1-x}\ M\ n^{4+}_x\ O_3$.

Table 4. Metal−Insulator Temperature Transition (T_{MI}), Room Temperature Resistivity (ρ_{300K}), Activation Energies (E_a), and Valence State of Mn^{x+} Ions for $Ca_{1-x}Ce_xMnO_3$

x	T_{MI} (K)	ρ_{300K} (Ω cm)	temperature range used for obtaining E_a (K)	E_a (meV)	Mn^{x+}
0.00		20.5	300−640	89.0	4.00
			660−870	342.2	
0.01	607	1.10	300−525	80.0	3.98
0.05	415	0.248	300−398	62.1	3.9
0.10	327	0.097	300−325	40.6	3.8
0.15		0.058			3.7
0.20	328	0.071	300−325	53.8	3.6
0.25	413	0.295	300−372	140.6	3.5

It was found that the resistivity below T_{MI} exhibits a thermally activated behavior for all the samples with $0.01 \le x \le 0.25$ except for $x = 0.15$ (see Figure 7), from which the activation energy E_a can be calculated listed in Table 4. According to our results, the conduction mechanism is via thermally activated small-polaron hopping between Mn^{3+} and Mn^{4+} localized states. The slight change in the slope of the temperature dependence of the conductivity for $x = 0$ at ~600 K (see Figure 7) was previously discussed in the literature.[24,33] Furthermore, our value for the activation energy, $E_a = 98.0$ meV, compares well with the value of 50 and 160 meV found by other workers for $x = 0$ synthesized by the same method as the present work[24] and by ceramic

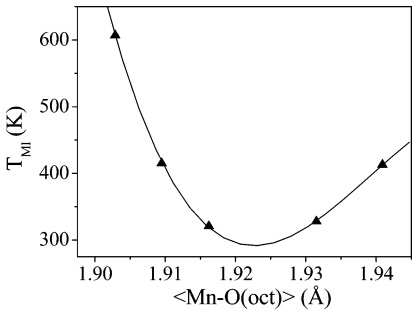

Figure 6. T_{MI} vs mean bond length ⟨Mn−O(oct)⟩ for the $Ca_{1-x}Ce_xMnO_3$ system.

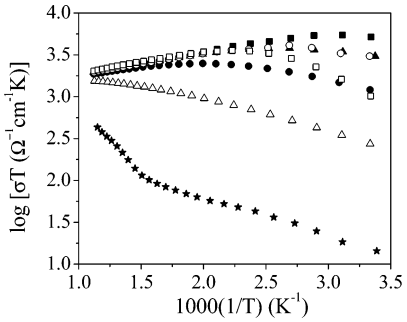

Figure 7. Plot of log (σT) vs 1000/T for $Ca_{1-x}Ce_xMnO_3$ ($0 \le x \le 0.25$). (★) $x = 0.00$, (△) $x = 0.01$, (●) $x = 0.05$, (▲) $x = 0.10$, (■) $x = 0.15$, (○) $x = 0.20$, (□) $x = 0.25$.

technique.[33] With the increase in Ce-substitution the activation energy for electrical conductivity is found to decrease linearly up to $x = 0.10$. For $x \ge 0.20$ a slight increase in activation energy is observed. The substitution of Ca^{2+} by Ce^{4+} should lead to a higher Mn^{3+} content with a consequent lowering of the energy barrier for polaron hopping, which lowers the activation energy for conduction.

Also, a similar evolution of the activation energies (E_a) in the low-temperature range 20−300 K has been reported earlier for $Ca_{1-x}Ce_xMnO_3$ samples ($x = \le 0.2$).[15] For $x \ge 0.075$ the authors verified an increase in the effective gap activation energy associated with entering the CO-ordered phase near 255 K with composition.

Our results of doping level dependence on the activation energy are in agreement with previous studies of $La_{1-x}Ca_xMnO_3$ thin films[30] where the authors concluded that the activation energy decreases monotonically as x is increased and the samples with $x = 0.83$ and 0.9 have the lowest activation energies suggesting that the more highly charged La^{3+} ions bind the polarons more tightly than Ca^{2+} ions.

This work leads to the conclusion, and according to what has been previously suggested,[34] that the structural and electrical properties of the $CaMnO_3$ based manganites are dominated by the charge state of Mn rather than by the size of the doping tetravalent cerium ion, since the A site mean ionic radius variation is very little (3.7%) compared with the decrease in the mixed valence state of Mn from 4 to 3.5 (12.5%).

Conclusions

This study shows the great influence of Ce-doping on the properties of $Ca_{1-x}Ce_xMnO_3$ manganites, i.e., the exceptional ability of cerium doping to induce a metal to insulator transition at high temperature in the manganite $CaMnO_3$. In the Ce-substituted phases the semiconducting $CaMnO_3$ changed to metallic behavior with a metal−insulator transition at high temperatures. The T_{MI} values are correlated with the degree of substitution, lattice effects, and valence state of manganese ions. Moreover, the change of metallic to semiconductor behavior at T_{MI} can be associated with the appearance of charge order transition at low temperature.

Our results indicate that the electron concentration introduced by doping plays a crucial role in the electrical conductivity of these materials. Hence, the structural and electrical properties of the $CaMnO_3$-based manganites are dominated by the charge state of Mn rather than by the size of the doping tetravalent cerium ion. These results suggest that the valence state of Mn plays a significant role in the T_{MI}, ρ_{300K}, and E_a values.

CM040188B

(33) Taguchi, H. *Phys. Status Solidi A* **1985**, *88*, K79.

(34) Raveau, B.; Maignan, A.; Martin, C.; Hervieu, M. *Chem. Mater*. **1998**, *10*, 2641.